Inductively Powered Pressure Sensing System Integrating a Far-Field Data Transmitter for Monitoring of Intracranial Pressure

M. Waqas A. Khan, *Student Member, IEEE*, Lauri Sydänheimo, *Member, IEEE*, Leena Ukkonen, *Member, IEEE,* Toni Björninen, *Member, IEEE*

***Abstract*—Monitoring of intracranial pressure (ICP) provides a life-saving diagnostic tool. We present a battery-free pressure sensing system for minimally invasive ICP monitoring. It comprises a cranially concealed wireless pressure sensor and on- and off-body external units. The sensor is based on a piezoresistive element and is inductively powered through an on-body unit. It is also equipped with a far-field antenna which conveys the pressure data to the off-body unit. We present the electromagnetic modelling of the system and report results from experiments carried out in a setting which mimics the biological operation environment. The simulation and measurement results demonstrate the wireless pressure monitoring at a distance up to one meter over the pressure range from −3 mmHg to 33 mmHg and assess the impact of an imperfectly aligned inductive link on the operation of the system.**

***Index Terms*— Intracranial Pressure (ICP), inductive power link, piezoresistive pressure sensor and far-field data transmitter.**

I. Introduction

Intracranial pressure (ICP) monitoring is required in management of various brain diseases and injuries [1-2]. The relation between ICP and the intracranial volume can be described as a pressure-volume curve. Due to the compensatory reserve, ICP does not vary much in the first part of the curve. After exceeding the compensatory reserve, there is a rapid rise in it. Normally, ICP depends on age and body posture but generally, for adult it is between 5 and 15 mmHg, for children between 3 and 7 mmHg and for infants between 1.5 and 6 mmHg [1-2]. In clinical practice, the pressure is commonly measured from the ventricular system of the brain through a catheter. This invasive approach, however, introduces the risk of hemorrhage and infection and is limited to short-term usage in the hospital environment. Hence, several studies [3-7] have focused on the development of non-invasive methods, where the pressure is sensed indirectly from the outside of the cranium. Although non-invasive methods are attractive due to placement simplicity and safety, they have two main limitations [1]. First, they lack in the accuracy as compare to invasive methods. Second, due to the anatomical variations, non-invasive methods cannot be used for large percentage of patients. [1]

An implantable system without any external wire connection is an alternative for ICP monitoring. In this type of system, an implanted sensor is wirelessly connected to an external unit. This helps to reduce the risk of infection by eliminating the need for puncturing the skin [3]. Study [8] presents a battery powered implant for ICP monitoring at industrial–scientific–medical (ISM) band of 2.45 GHz. However, the main limitations of a battery powered ICP monitoring system are: large size (due to the large size of the battery) and life-time (which depends on battery life-time). Passive implants have also been reported in the literature [9-12]. However, here the attainable wireless link distance is limited in comparison with a battery-powered system. Recently, reference [13] presented the wireless power supply with hybrid super-capacitor and battery storage for ICP monitoring devices.

In contrast, the ICP monitoring system presented in this work is based on a battery-free wirelessly powered pressure sensor placed under the skull. This is a potential minimally invasive solution to overcome the limited wireless link distance of the fully passive approach, and life-time and size limitations of the battery assisted approach. This work is continuation of our previous studies [14-15], where we activated the pressure sensor wirelessly and presented the pressure readout results. In the previous work, the pressure readout has been done in the air through wires by monitoring the output voltage of the pressure sensor.

In this article, we present a complete pressure sensing system consisting of in-, on-, and off-body units. The pressure sensor placed under the skull is powered by the on-body unit through inductive coupling. After activation, it monitors the pressure and transmits the pressure readout directly to the off-body unit through a far-field antenna. Fig. 1(a) presents the system level description of the pressure sensing system. A piezoresistive pressure sensor is used to monitor the pressure. The pressure sensor has two input and two output terminals.

Manuscript submitted on October 3rd, 2016 and revised on December, 12th, 2016 and on 25th Jan, 2017. This research was funded by Academy of Finland, Jane and Aatos Erkko Foundation, TEKES and Nokia Foundation.

M. Waqas A. Khan, Lauri Sydänheimo, Leena Ukkonen and Toni Björninen are with the Faculty of Biomedical Sciences and Engineering, Tampere University of Technology and Institute of Bioscience and Medical Technology (BioMediTech), Tampere, Finland (e-mail: {muhammad.khan, toni.bjorninen, leena.ukkonen, lauri.sydanheimo}@tut.fi).

The differential output voltage of the pressure sensor is sensitive toward change in the pressure. The output voltage of the pressure sensor is amplified through an amplifier and drives the voltage control oscillator (VCO). Finally, the output of the VCO is connected to a far-field antenna transmitting the monitored pressure in ISM band of 2.45 GHz. It is important to note that the in-body unit has two wireless modalities: it integrates a 2-turns coil antenna and a far-field antenna which are used to pick up energy from on-body unit (inductive coupling) and to transmit the pressure readout to off-body unit (propagating EM waves), respectively. To avoid any confusion, we will use the following terminologies to represent different antennas in the pressure sensing system: 2-tuns coil antenna (in-body unit), far-field antenna (in-body unit), 2-turns loop antenna (on-body unit) and $\lambda/2$ dipole antenna (off-body unit).

The remainder of the paper is organized in five sections. Next Section explains the design and the simulation of the wireless link and the antennas. Section III discusses the measurement setup and the results. Impact of misalignment in the inductive link is analyzed in Section IV and finally Section V presents conclusions and future work.

II. System Design and Simulation

Our system consists of in-, on-, and off-body units as illustrated in Fig. 1. The in-body unit contains a 2-turns coil antenna, a matching circuit, a rectifier, a charge storage super-capacitor, a zener diode, a piezoresistive pressure sensor, an amplifier, a VCO and a far-field antenna. The on-body unit consists of a 2-turns loop antenna and a matching circuit. The off-body unit consists of a $\lambda/2$ dipole antenna connected to the spectrum analyzer.

A. Modelling of Wireless Link

We used the anatomical head model provided in ANSYS HFSS v15 to model the antennas and the wireless link in a biological environment. As shown in Fig. 1(b), the 2-turns loop antenna of the on-body unit is placed at a distance of 5 mm from the skin and the 2-turns coil antenna of the in-body unit is placed in the cerebrospinal fluid (CSF). Moreover, the separation between the antennas is 16 mm. From the simulation of the coupled antenna system, we obtained two-port Z-parameters and computed the maximum link power efficiency of the system, which is given by

$$G_{p,max} = \frac{|z_{21}|^2}{a + \sqrt{a^2 - |z_{12}z_{21}|^2}}, \qquad (1)$$

where $a = 2\mathrm{Re}(z_{11})\mathrm{Re}(z_{22}) - \mathrm{Re}(z_{12}z_{21})$. It is determined by the internal electromagnetic properties of the system: structure of the antennas, coupling and materials. Impedance matching is an external property and excluded from this figure of merit.

The power fed into the 2-turns loop antenna is limited by the human safety limits given in terms of the Specific Absorption Rate (SAR). We have followed the U.S. Federal Communications Commission (FCC) regulation which limits the SAR averaged over one gram of tissue to SAR_{max} = 1.6 W/kg. In Fig. 1(b), skin is the one closest to 2-turns loop antenna and we found that the maximum of the local SAR occurred on its surface, which is facing the 2-turns loop antenna. However, the thickness of skin is less than the edge of an averaging cube containing one gram of skin (the average density of 1.109 g/cm^3 [16]) which is approximately 9.7 mm. Thus, to ensure numerical stability and reproducibility of the data, we estimate SAR using another model where the 2-turns loop antenna alone is placed at an equal distance from 18.75´ 18.75´ 30 cm^3 block of skin. Given that SAR is proportional to the power delivered into the 2-turns loop

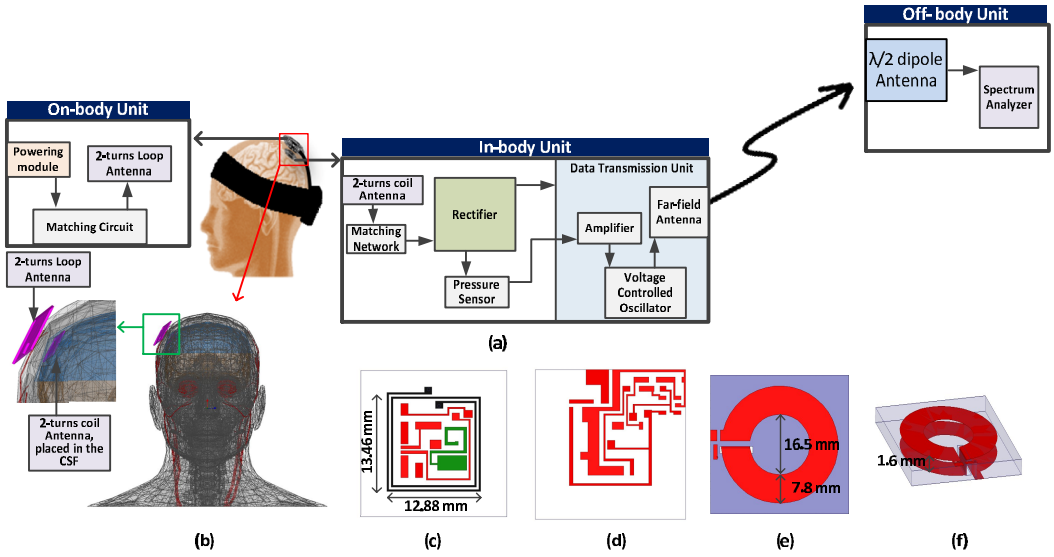

Fig. 1. (a) System level description of the pressure sensing system for wireless ICP monitoring (b) anatomical human head model in ANSYS HFSS v15 for wireless link and antenna modeling (c) front side of in-body unit consists of 2-turns coil antenna (black), far-field antenna (green) and traces for other components (red) (d) backside of in-body unit consists of traces for electronic components (e) top view of on-body unit antenna (f) side view of on-body unit antenna

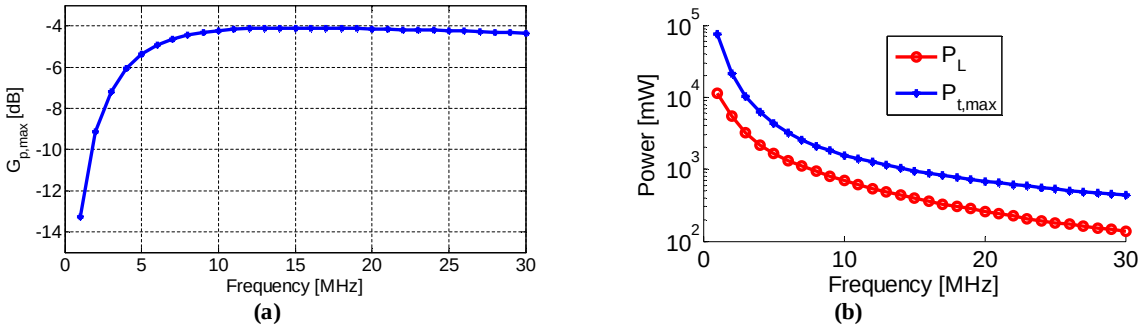

Fig. 2. (a) Link power efficiency ($G_{p,max}$) (b) maximum SAR-compliant transmission power ($P_{t,max}$) and power delivered to the in-body unit antenna load (P_L) under conjugate-matched conditions

antenna, we have

$$\frac{SAR}{tP_{test}} = \frac{SAR_{\max}}{P_{t,\max}}; t = \frac{4 \times 50W \times \mathrm{Re}(Z_{ext})}{|50W + Z_{ext}|^2}, \qquad (2)$$

where P_{test} = 1 W is the power available from a 50 Ω test source in HFSS, $P_{t,max}$ is the power delivered to the 2-turns loop antenna which generates SAR_{max} in the skin block, and τ is the power transfer efficiency between the test source and the 2-turns loop antenna (impedance: Z_{ext}). Hence, we find the maximum power available for a load connected to the coil antenna in the in-body unit to be $P_L = P_{t,max}\, G_{p,max}$, where $P_{t,max}$ is solved from (2) and $G_{p,max}$ is given in (1).

B. Antenna Designing

The on-body unit contains the 2-turns loop antenna presented in [17-18]. Due to structural properties of the 2-turns loop antenna, it can transmit more power with low and uniform SAR by maintain the same link power efficiency compared with a single-turn loop antenna. Fig. 1 (e) and (f) shows the top and side view of the 2-turns loop antenna. The antenna is designed on FR4 substrate with the inner diameter of 16.5 mm and the trace width of 7.8 mm. The gap between the two loops is 1.6 mm, which is equal to the height of the substrate.

The in-body unit has two antennas, a 2-turns coil antenna and a far-field antenna. Both antennas are designed on a flexible polyimide substrate with dielectric constant (ε_r) of 3.3, tangent loss (tanδ) of 0.002 and thickness of 50 μm. Fig. 1(c) shows the front side of the in-body unit, which contains a 2-turns coil antenna and a far-field antenna. The front side of the in-body unit is facing toward the on-body unit. Fig. 1(d) shows the backside of the in-body unit. The circuit board is designed on the backside for attachment of pressure sensor and other components. The detail of the far-field antenna is presented in [19]. Similarly, the detail of 2-turns coil antenna is presented in [14]. For biocompatibility, in-body unit is encapsulated with silicone and Parylene C coating (details in Section III). Therefore, the same coating is added in the simulation model.

The off-body unit consists of a $\lambda/2$ dipole antenna. It is designed for ISM band of 2.45 GHz. The received signal of

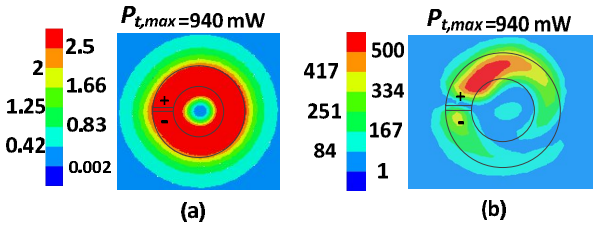

Fig. 3. (a) Local SAR (W/kg) distribution on the skin when maximum allowed power is transmitted at 15 MHz (b) Local E-field (V/m) distribution on the skin when maximum power is transmitted at 15 MHz

TABLE I
SIMULATED Z-PARAMETER OF 2-PORT NETWORK AT 15 MHZ

Z-Parameter	Value [Ω]
z_{11}	0.052743 + 9.246686i
z_{12}= z_{21}	0.019429 + 0.444737i
z_{22}	0.907672 + 12.235319i

$\lambda/2$ dipole antenna is recorded in the spectrum analyzer for monitoring the variation in the pressure.

C. Simulation Results

Fig. 2(a) shows the simulated link power efficiency ($G_{p,max}$), maximum SAR-compliant transmission power ($P_{t,max}$) and power delivered to the in-body unit antenna load (P_L) under conjugate-matched conditions. The simulation results shows that the maximum of $G_{p,max}$ occurs at 15 MHz. Table I shows the simulated Z-parameter of 2-port network at 15 MHz.

$P_{t,max}$ and P_L are large at lower frequency and decrease as the frequency increases (see Fig. 2(b)). Even though at lower frequency $P_{t,max}$ is large, $G_{p,max}$ is small which would result in large power consumption. This is the reason we want to operate the system at a frequency with larger $G_{p,max}$ value. Fig. 3 shows the local SAR and the E-field distribution on the skin when $P_{t,max}$ is transmitted at 15 MHz. Because of the external antenna structure, SAR is uniformly distributed. Moreover, one terminal of the feeding port has greater distance from the skin compared to the other that is why it has only one E-field peak as explained in [17-18].

III. MEASUREMENT AND DISCUSSION

After design and simulation, all of the system blocks shown

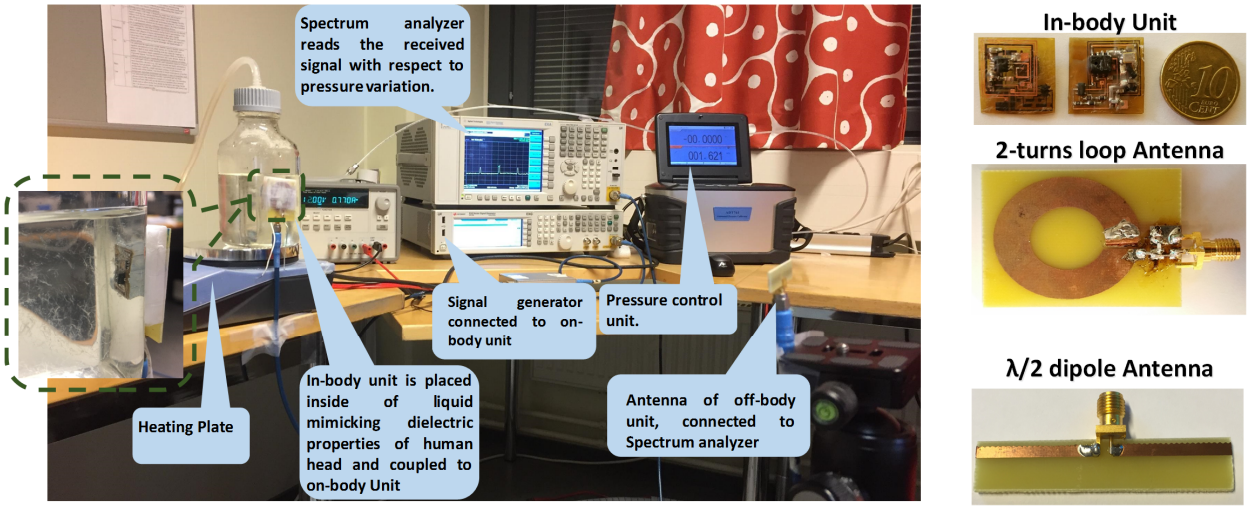

Fig. 5. The measurement setup and fabricated in-body unit, 2-turns loop antenna of on-body unit and λ/2 dipole antenna of off-body unit.

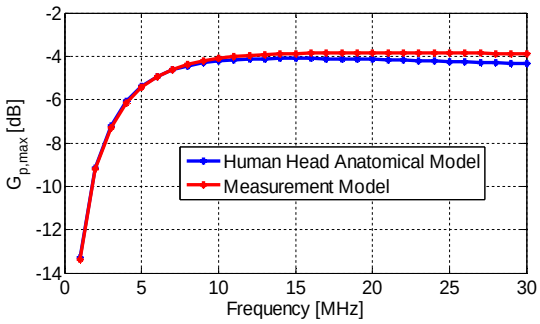

Fig. 4. Comparison between simulated $G_{p,max}$ for the human head anatomical ANSYS HFSS and the measurement models.

in Fig. 1 are fabricated. As a matching network, an LC-matching configuration is used for 2-turns loop antenna, whereas a capacitor in the parallel configuration is used for 2-turns coil antenna.

In the in-body unit, two Schottky diodes (Skyworks SMS7630 series) along with two 1 µF capacitors in the charge pump configuration are used as a rectifier for RF-to-DC conversion. A super-capacitor (CPH3225A) of 11 mF along with a zener diode are used to stabilize the voltage to around 3 V. A piezoresistive pressure sensor (Amphenol NPP301A-200A) with 5000 Ω input resistance is connected after the zener diode. The output of the pressure sensor is connected to the input of the amplifier (LT6003) and drives the VCO (MAX2750). The VCO output is connected to the far-field antenna. The circuit designing is done in NI Multisim 13.0 software.

A. Measurement Setup

We perform three different measurements. The first of these is S-parameter of the wireless link, second is pressure readout from the pressure sensing system and third is misalignment between inductively coupled antennas. The pressure sensing system performance toward the change in the pressure is measured in a liquid mimicking the dielectric properties of the human head. In measurement setup, we used a different measurement model compared to the anatomical head model provided in ANSYS HFSS v15. In our system, there are two communication links. First of these is a wireless power link and second is a far-field link to transfer the monitored pressure. In the wireless power link, the material in-between the coupled antennas is important [20]. However, in the far-field link, the far-field antenna is designed for human head environment [19]. That is why it should be placed in an environment close to human head for its normal operation. Moreover, in the targeted application of ICP monitoring, the in-body unit is going to be placed in CSF. This makes also important the testing of the in-body unit in a liquid mimicking the dielectric properties of human head.

For the wireless power link, we placed a pig skin of 6 mm in-between the coupled antennas (2-turns coil and 2-turns loop antennas). In the measurement, there is a gap of 16 mm (4 mm air + 6 mm pig skin + 4 mm glass + 2 mm liquid mimicking human head properties) between the coupled antennas, and both antennas are centrally aligned. The skin has larger losses compared with fat and bone [18]. That is why, we used only skin in the measurement to study the worst case scenario. Fig. 4 shows the simulated $G_{p,max}$ for the anatomical head model and the measurement model. The results from two models are in good agreement at our interested frequency of 15 MHz.

For the far-field link, we place the in-body unit in a liquid mimicking the human head properties. We follow IEEE standard for head properties (at 2.45 GHz, ε_r = 39.2 and σ = 1.8 S/m). The liquid phantom is made of water, sugar and salt as explained in [19]. Relative permittivity of water is reduced by adding sugar, whereas adding salt increases conductivity. At 2.45 GHz, the measured liquid properties are: ε_r = 39.5 and σ = 2.65 S/m [19].

Fig. 5 shows the measurement setup and the fabricated 2-turns loop antenna, $\lambda/2$ dipole antenna and the in-body unit. The in-body unit is placed inside the glass bottle filled with liquid mimicking dielectric properties of human head (see Fig. 5). The pressure inside the glass bottle is controlled with pressure controlling device ADT761 that generates pressure with high precision. Moreover, the body temperature (37 ^{o}C) is maintained by placing the glass bottle on a heating plate.

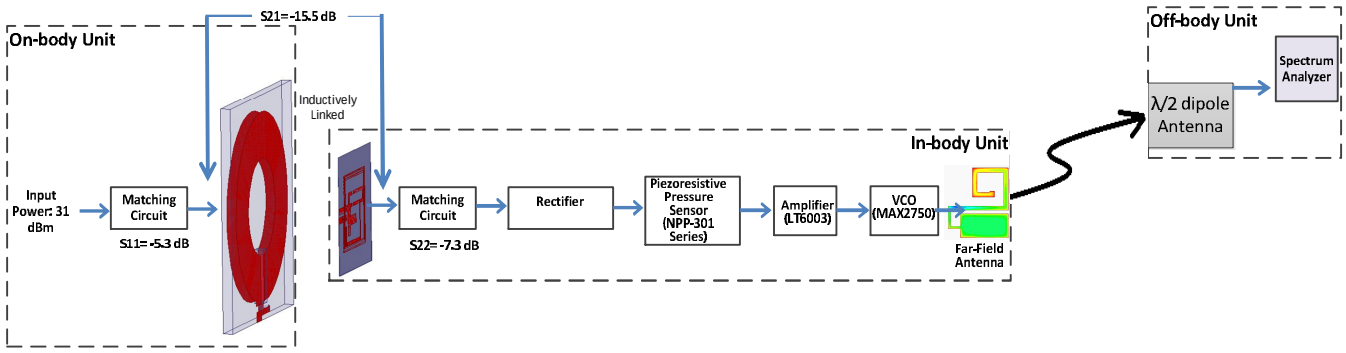

Fig. 6. Measured S-parameters and power transfer of the system.

For biocompatibility, we have used two layers of coating. Initially, the in-body unit is coated with biocompatible MED-2000 silicone adhesive with total thickness of 1 mm. Afterward, it is coated with 2 µm Parylene C which is a vapor deposited polymer and produces uniform and pin-hole free coating.

B. S-Parameter and Power Transfer Measurement

We measure the S-parameters through Vector Network Analyzer (VNA). The port 1 of the VNA is connected to 2-turns loop antenna and port 2 to 2-turns coil antenna. The SMA connectors are soldered to both antennas. Both antennas are centrally aligned and separated with 16 mm distance. After S-parameter measurement, the 2-turns loop antenna of the on-body unit is fed with 31 dBm of input power. This activates the pressure sensor. Fig. 6 shows the measured S-parameters and the power transfer. The measured transmission loss between the antennas is 15.5 dB. The reflection coefficients for 2-turns loop antenna and 2-turns coil antenna are –5.3 dB and –7.3 dB respectively. Small loop antennas at lower frequency are difficult to match to 50 Ω because their input impedances have small real part. The transmission loss in our system can further be reduced by improving the matching network. We are able to deliver 15.5 dBm of power to the in-body unit with system power transfer efficiency of –15.5 dB (2.81%). The fed power to the 2-turns loop antenna is 31 dBm (1.26W). However, the reflection coefficient for 2-turns loop antenna is –5.3 dB. This means that 889 mW power is coupled to in-body unit. From Fig. 2 (b), the maximum SAR-compliant transmission power ($P_{t,max}$) is 940 mW at 15 MHz. Thus, the results demonstrate that the sensor is activated within SAR-compliant transmission power.

We computed the $G_{p,max}$ from measured S-parameters after compensating the loss due to the matching components. The loss is compensated through simulated insertion loss of conjugate-matched matching networks. Thus, the measured and the simulated $G_{p,max}$ values are –4.54 dB and –3.8 dB respectively at 15 MHz.

C. Pressure Change Measurement

In the second measurement, we perform the pressure change readout experiment. The pressure inside the glass bottle is increased/decreased with pressure controlling unit ADT761. The pressure is changed in both Up (–3 mmHg to 33 mmHg)

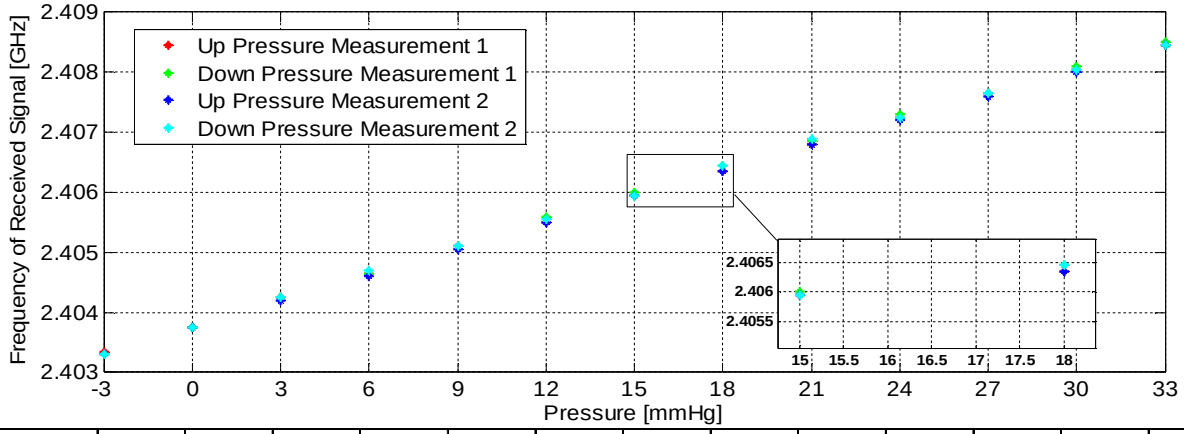

Minimum Frequency [GHz]	2.4033	2.40375	2.4042	2.4046	2.40505	2.4055	2.40595	2.40635	2.4068	2.4072	2.4076	2.408	2.40845
Maximum Frequency [GHz]	2.40335	2.40375	2.40425	2.4047	2.4051	2.4056	2.406	2.40645	2.4069	2.4073	2.40765	2.4081	2.4085

Fig. 7. Measured frequency of the received signal with change in the pressure.

and Down (33 mmHg to –3 mmHg) directions with 3 mmHg step size. Thus, we are able to study the pressure sensing system behavior in both directions. Moreover, we perform two sets of Up/Down measurements to verify the repeatability of the pressure sensing system. To verify the temperature stability during the measurement, we measure the liquid temperature before and after the measurement. The temperature values are 37.1 ºC and 36.6 ºC before and after the measurement respectively.

Fig. 7 shows the measured frequency of the received signal from the in-body unit versus change in the pressure. Firstly, it is evident that the pressure sensing system response is linear over the studied pressure range. A total of 5.2 MHz change in the frequency of the received signal (from 2.40330 GHz to 2.40850 GHz) is observed corresponding to 36 mmHg change in the pressure (from –3 mmHg to 33 mmHg). This means that there is 145 kHz change in the frequency of the received signal for 1 mmHg change in the pressure. Secondly, the pressure sensing system showed an excellent repeatability with an average hysteresis of only 150 kHz between the increasing and decreasing pressure. Fig. 7 also shows the maximum and the minimum measured frequency values of the received signal. Based on these results, it can be concluded that pressure sensing system has a resolution of 2 mmHg. The reference [11] has reported results in an experimental setup closed to ours. Moreover, the reported resolution of the system in [11] is 2.5 mmHg. This means that presented system in this article has pressure sensing resolution comparable with results presented in reference [11].

IV. Misalignment Study for Wireless Link

The power transfer efficiency in an inductive link between the antennas depends on their size, structure, separation, alignment and properties of material between them [20]. We are using inductive coupling for powering the analog piezoresistive pressure sensor. This makes important to study the pressure readout error due to misalignment between the coupled antennas.

In misalignment measurement, as shown in Fig. 8, we vary the ‘X’ and ‘Y’ from –2 mm to 2 mm with a step size of 2 mm on a rectangular coordinate axis. During the measurement, the separation of the antennas and input power of the 2-turns loop antenna were kept constant at 16 mm and 31 dBm respectively. We measured a total of eight points. Fig. 8 shows the measured shift in the frequency of the receive signal with respect to the centrally aligned case and estimated error in the pressure readout. In Fig. 8, bigger loop represents the 2-turns loop antenna whereas smaller loop represents the 2-turns coil antenna. From Fig. 7, it is clear that there is total 5.2 MHz shift in frequency of the received signal with 36 mmHg change in the pressure. This means that 145 kHz of frequency shift corresponds to 1 mmHg change in the pressure. Based on this information, we are able to calculate the error in the pressure readout due to misalignments. For example, at X= –2 and Y= 0, there is 630 kHz shift in the frequency of the received signal from the in-body unit which is more than four times of 145 kHz. This means that there is an extra 5 mmHg

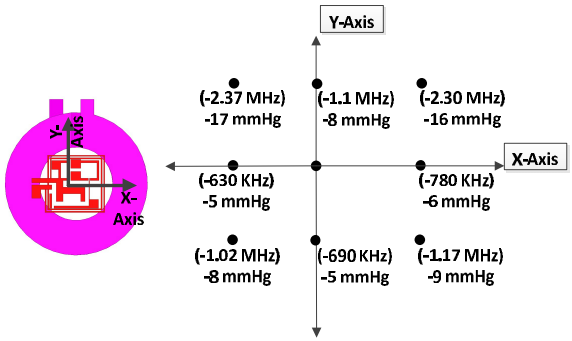

Fig. 8. Measured shift in the frequency of the received signal and the estimated error in the pressure readout for different X and Y values.

error in the pressure readout induced due to misalignment between the antennas. The negative sign indicates that the recorded pressure is 5 mmHg less than the actual pressure value. Similarly, the negative sign of the frequency shift indicates that the received signal frequency is 630 kHz less compared to the centrally aligned case.

After comparing the studied cases of Fig. 8, we can conclude that misalignment in the inductive link has significant effect on the pressure readout accuracy. Yet, as can be seen, all of the misaligned pressure values are lower than the centrally aligned case. This means that misalignment always results in lower pressure values compare to the actual. Thus, in practice, alignment can be achieved by moving the on-body unit to the location corresponding to maximum pressure.

The reason for the deviation in the pressure readout due to misalignment is that the external 2-turns loop antenna has very strong H-field in the middle, but it decays sharply when moving away from the center. Moreover, both 2-turn coil and 2-turns loop antennas are comparable in size and tightly coupled. Because of the sharp decay of H-field, the voltage at in-body unit drops significantly. As a result, it induces large pressure error. To mitigate this impact, a topic in our ongoing work is the optimization of the antenna of the on-body unit for more uniform magnetic field distribution in larger area.

V. Conclusion

We presented a battery-free wirelessly powered pressure sensing system for intracranial pressure (ICP) monitoring. The on-body unit powers the pressure sensor through inductive coupling and monitored pressure is transmitted through a far-field data transmission unit. The transmitted pressure signal is received by off-body unit placed at 1 m distance. A 31 dBm power is fed to the on-body unit and the in-body unit receives 15.5 dBm with total system power transfer efficiency of 2.82 %. The pressure sensing system operability is attested in an environment mimicking the dielectric properties of human head. Moreover, the pressure sensing system shows good repeatability and bi-directional pressure readout performance. Finally, our study shows that misalignment between the coupled antennas has significant effect on the pressure readout accuracy. This could be solved by taking multiple readings and filtering out the maximum pressure value. Our future step is to minimize the pressure readout error due to misalignment

by optimizing the antenna of the on-body unit and to study the pressure sensing system drift.

REFERENCES

[1] P. H. Raboel, J. Bartek, M. Andresen, B. M. Bellander, B. Romner, "Intracranial pressure monitoring: invasive versus non-invasive methods – a review," *Crit. Care Res. Pract.*, vol. 2012, article ID: 950393, Mar. 2012.

[2] M. Smith, "Monitoring intracranial pressure in traumatic brain injury," *Anesth. Analg.*, vol. 106, no. 1, pp. 240–248, Jan. 2008.

[3] J. Zhong, M. Dujovny, H. K. Park, E. Perez, A. R. Perlin, and F. G. Diaz, "Advances in ICP monitoring techniques, " *Neurological research* 25.4, pp. 339-350, Jun. 2003.

[4] R. Ravi, R. J. Morgan, "Intracranial pressure monitoring" *Current Anaesthesia & Critical Care*, vol. 14, issues 5–6, pp. 229-235, Dec. 2003.

[5] N. Ross, C. A. Eynon, "Intracranial pressure monitoring," *Neuro Intensive Care*, vol. 16, issue 4, pp. 255–261, 2005.

[6] Headsense, "Headsense," http://www.head-sense-med.com/. [Site accessed on 9.12.2016]

[7] F. M. Kashif, G. C. Verghese, V. Novak, M. Czosnyka, T. Heldt. "Model-based noninvasive estimation of intracranial pressure from cerebral blood flow velocity and arterial pressure," *Sci Transl Med* 4: 129ra44, Apr. 2012

[8] U. Kawoos, M.-R. Tofighi, R. Warty, F. A. Kralick, A. Rosen, "In-vitro and in-vivo trans-scalp evaluation of an intracranial pressure implant at 2.4 GHz," *IEEE Trans. Microw. Theory Techn.*, nol. 56, no. 10, pp. 2356–2365, Oct. 2008.

[9] Mems-iss.com, 'Wireless Intracranial Pressure Monitor (WIPM)'. [online]. http://mems-iss.com/wipm/ [Site accessed on 9.12.2016]

[10] Raumedic.com,'Telemetric ICP Measurement'. [online] https://www.raumedic.com/hospital-care/neuromonitoring/telemetry/ [Site accessed on 9.12.2016]

[11] Mohammad H. Behfar, E. Moradi, T. Björninen, L. Sydänheimo, L. Ukkonen, "Biotelemetric wireless intracranial pressure monitoring: an in vitro study," *Intl. J. Antennas Propag*., vol. 2015, Article ID 918698, 10 pages, Nov. 2015.

[12] L. Y. Chen, B. C.-K. Tee, A. L. Chortos et al., "Continuous wireless pressure monitoring and mapping with ultra-small passive sensors for health monitoring and critical care," *Nature Communications*, vol. 5, article 5028, Oct. 2014.

[13] A. P. Hu, Y. W. You, F. Y. B. Chen, D. McCormick and D. M. Budgett, "Wireless power supply for ICP devices with hybrid supercapacitor and battery storage," *IEEE Journal of Emerging and Selected Topics in Power Electronics*, vol. 4, no. 1, pp. 273–279, Mar. 2016.

[14] M. W. A. Khan, T. Björninen, L. Sydänheimo, L. Ukkonen, "Remotely Powered Piezoresistive Pressure Sensor: Toward wireless monitoring of intracranial pressure," *IEEE Microwave and Wireless Components Letters* , vol. 26, no. 7, pp.549-551, Jul. 2016.

[15] M. W. A. Khan, T. Björninen, M. Rizwan, L. Sydänheimo and L. Ukkonen, "Piezoresistive pressure sensor for ICP monitoring: remote powering through wearable textile antenna and sensor readout experiment," *IEEE AP-S/URSI*, Jun. 2016.

[16] Itis.ethz.ch, "Tissue Properties" [online] http://www.itis.ethz.ch/virtual-population/tissue-properties/database/density [Site accessed on 9.12.2016]

[17] M. W. A. Khan, T. Björninen, L. Sydänheimo and L. Ukkonen, "Two-turns antenna and magnetic materials for effective powering of mm-size implant in wireless brain-machine interface system," *IEEE IMWS-BIO Dig.*, p.134-135, Sept. 2015.

[18] M. W. A. Khan, T. Björninen, L. Sydänheimo, L. Ukkonen, "Characterization of two-turns external loop antenna with magnetic core for efficient wireless powering of cortical implants," *IEEE Antennas Wireless Propag. Lett.*, vol. 15, pp. 1410–1413, Apr. 2016.

[19] M. W. A. Khan, E. Moradi, L. Sydänheimo, T. Björninen, Y. Rahmat-Samii, L. Ukkonen, "Miniature co-planar implantable antenna on thin and flexible platform for fully wireless intracranial pressure monitoring system," *Intl. J. Antennas Propag*., vol. 2017, Article ID 9161083, 9 pages, 2017.

[20] A. K. RamRakhyani, S. Mirabbasi, and M. Chiao, "Design and optimization of resonance-based efficient wireless power delivery systems for biomedical implants," *IEEE Trans. Biomed. Circuits. Syst*., vol. 5, no. 1, pp. 48–63, Feb. 2011.

M. Waqas A. Khan (S'15) received the BE electronics engineering degree from the National University of Sciences and Technology, Islamabad, Paksitan in 2008, the M. Sc. degree in electrical engineering with major in RF electronics (antennas) from the Tampere University of Technology, Tampere, Finland, in 2014, where he is currently pursuing the Ph.D. degree in Wireless Identification and Sensing Systems Research Group.

He has been a RF Engineer for Mobilink Pakistan and a RF Optimization Engineer for Huawei project of Pak Telecom Mobile Limited (PTML) Pakistan. His research areas include antenna designing, electromagnetic modelling, implantable biomedical systems, RFID systems and low-profile antennas.

Lauri Sydänheimo (M'02) received the M.Sc. and Ph.D. degrees in electrical engineering from the Tampere University of Technology (TUT), Tampere, Finland.

Currently, he is a Professor at Faculty of Biomedical Sciences and Engineering, TUT. He has authored more than 200 publications in radio-frequency identification (RFID) tag and reader antenna design and wireless system performance improvement. His current research interests include wireless data communication and wireless identification and sensing

Leena Ukkonen (M'04) received the M.Sc. and Ph.D. degrees in electrical engineering from Tampere University of Technology (TUT), Tampere, Finland, in 2003 and 2006, respectively.

Currently, she is a Professor and Academy Research Fellow with the Faculty of Biomedical Science and Engineering, Tampere University of Technology (TUT), Tampere, Finland, and is leading the Wireless Identification and Sensing Systems Research Group.

Toni Björninen (M'09) received the M.Sc. and doctoral degrees in Electrical Engineering in 2009 and 2012, respectively, from Tampere University of Technology (TUT), Tampere, Finland.

He is currently an Academy of Finland Research Fellow in the Faculty of Biomedical Sciences and Engineering in TUT and a member of Institute of Biosciences and Medical Technology (BioMediTech). He has been a Visiting Postdoctoral Scholar in Berkeley Wireless Research Center in UC Berkeley and in Microwave and Antenna Institute in Electronic Engineering Dept., Tsinghua University, Beijing. His research focuses on technology for wireless health including implantable and wearable antennas and sensors, and RFID-inspired wireless systems. Dr. Björninen is an author of

123 peer-reviewed scientific publications. He is an Associate Editor in IET Electronics Letters and Editor in International Journal of Antennas and Propagation.